Available online at www.sciencedirect.com

SciVerse ScienceDirect

journal homepage: www.elsevier.com/locate/acme

Original Research Article

Theoretical and experimental study on the flattening deformation of the rectangular brazen and aluminum columns

Abbas Niknejad[a,*], *Seyed Mohammad Elahi*[a], *Seyed Ahmad Elahi*[a], *Seyed Ali Elahi*[b]

[a]*Mechanical Engineering Department, Yasouj University, P.O. Box 75914-353, Yasouj, Iran*
[b]*Mechanical and Aerospace Engineering Department, Shiraz University of Technology, Shiraz, Iran*

ARTICLE INFO

Article history:
Received 29 August 2012
Accepted 21 April 2013
Available online 25 April 2013

Keywords:
Energy method
Lateral compression
Column
Energy absorption
Thin-walled structure

ABSTRACT

This paper presents a theoretical and experimental study on lateral compression of square and rectangular metal columns. Some theoretical relations are derived to predict the absorbed energy, the specific absorbed energy and the instantaneous lateral load during the lateral compression. Analytical relations are obtained in two stages: elastic and plastic parts. In the plastic zone, the total absorbed energy by the column is calculated, based on the energy method. Then, an analytical equation is derived to predict the instantaneous lateral load. In the elastic part, the instantaneous load is obtained by linear behavior assumption. To verify the theoretical formulas, some lateral compression tests were carried out on square and rectangular columns and the experimental results are compared with the theoretical predictions, which shows a good agreement. Also, based on the experiments, effects of geometrical dimensions and material properties of the columns on the energy absorption capability are investigated. The results show that the absorbed energy by a column increases proportional to the column length. Also, columns with the thicker wall have the higher specific absorbed energy and so, rectangular columns with the thicker wall are the better energy absorbers during the flattening process. Also, the absorbed energy increases when the length of the column edge along which the load is applied decreases. Also, it is found that the specific absorbed energy by the aluminum columns is higher than the brazen ones and therefore, flattened columns with the high ratio of the flow stress/density are the better energy absorbers.

1. Introduction

The function of an energy absorber is absorbing the kinetic energy and dissipating it in some other forms of energy, ideally in an irreversible manner. Non-recoverable (inelastic) energy can exist in various forms such as plastic deformation, viscous energy and friction or fracture energy. Circular or square sectioned tubes are one of the most commonly used structural

*Corresponding author. Tel.: +98 741 222 9889; fax: +98 741 222 1711.
E-mail address: Aniknejad@mail.yu.ac.ir (A. Niknejad).

1644-9665/$ - see front matter © 2013 Politechnika Wrocławska. Published by Elsevier Urban & Partner Sp. z o.o. All rights reserved.
http://dx.doi.org/10.1016/j.acme.2013.04.008

elements due to their prevalent occurrence and easy manufacturability. For example, circular tubes can dissipate elastic and inelastic energy through different modes of deformation. Such methods of deformation include lateral compression, lateral indentation, axial crushing, splitting and tube inversion. Energy absorption characteristics and mean crushing loads of the mentioned deformations are important in viewpoint of applications and design of the safe machines. Such practical cases may consist of energy absorbers in the aircraft, automobile and spacecraft industries, nuclear reactors, steel silos and tanks for safe transportation of solids and liquids [1]. Gupta and Khullar [2] investigated collapse load of aluminum and mild steel tubes with square and rectangular cross-sections between parallel rigid platens. They showed that when one or all of the geometric imperfections are large, the tubes collapse at loads much smaller than the buckling load. But, when their geometric shapes are nearly true, the tube collapses at the buckling load. Gupta and Abbas [3] presented a detailed experimental investigation of the quasi-static lateral crushing of composite cylindrical tubes between flat platens. The metallic tubes fail by plastic buckling; however, the GFRE tubes collapse by a combination of fracture processes. Gupta et al. [4] introduced experimental and computational investigations of deformation and energy absorption behavior of rectangular and square tubes under lateral compression. A finite element model of lateral compression of the tubes was proposed. The predictions of simulated model were compared with experiments that showed a good agreement. Zeinoddini et al. [5] described an experimental study in which axially pre-loaded tubes were examined under lateral dynamic impact loads. The experimental tests showed that pre-loading has a substantial effect on the level of damage in tubes subjected to lateral impacts. Karamanos and Eleftheriadis [6] examined the collapse of tubular members under lateral loads in the presence of pressure. In particular, it emphasizes on the effects of external pressure on the ultimate load and the energy absorption capacity. It is found that the presence of internal pressure increases both the ultimate load and the energy absorption capacity. Liu et al. [7] presented an experimental and numerical study on the dynamic behavior of ring systems subjected to pulse loading. Experiments for the stress wave propagation in ring systems were performed using a modified split Hopkinson pressure bar test system. Numerical simulations of the stress wave propagation in the ring systems were conducted by using LS-DYNA. The numerical results showed a reasonable agreement with the experimental results. Karamanos and Andreadakis [8] examined the structural response of tubular members subjected to lateral quasi-static loading, imposed by wedge shaped denting devices, in the presence of internal pressure. Based on numerical study, it was concluded that the presence of internal pressure causes a substantial increase of the denting resistance force. Morris et al. [9] numerically and experimentally investigated the quasi-static lateral compression of nested systems with vertical and inclined side constraints. Different variations of external constraints were used as a means of increasing the energy absorbing capacity of the nested systems. The numerical results showed a reasonable correlation, comparing with the corresponding experiments. Niknejad et al. [10–12] investigated the energy absorption capability of the metal columns with circular, square and rectangular cross-sections under the axial loading and then, studied the effects of polyurethane foam-filler on mechanical behavior of specimens. Then, Niknejad et al. [13] investigated the effects of polyurethane foam-filler on the lateral plastic deformation of the circular tubes under radial quasi-static loading. Experimental results showed that the polyurethane foam-filler increases the lateral load during the compression tests and this effect in thinner tubes is more than thicker specimens. Nemat-Alla [14] introduced a simple technique and based on an inverse analysis, he predicted the hoop stress–strain behavior of tubes by using lateral compression test. Also, a finite element simulation of the quasi-static lateral compression of tubes between two rigid flat platens was carried out using the estimated stress–strain curve. To confirm theoretical predictions of the stress–strain curves, some uniform compression tests were carried out under the same testing conditions. Fan et al. [15] conducted desirable experiments to investigate the lateral crushing behavior of double-walled tubes with aluminum foam-filler. Sandwich tubes with different diameter to thickness ratios were laterally compressed. To validate the numerical solutions by ABAQUS/Explicit, the corresponding experimental results were performed. Different crushing patterns were revealed and classified. Hall et al. [16] carried out some lateral compression tests on aluminum foam-filled tubes with circular cross-section. They performed the flattening tests with the different strain rates and indicated that the results are not strain-rate dependent. Abosbaia et al. [17] considered behavior of segmented woven roving laminated composite tubes subjected to quasi-static lateral loading. Experimental measurements showed that the segmented composite tubes consisting of cotton fiber/epoxy and carbon fiber/epoxy are particularly efficient crush elements. Mahdi and Hamouda [18] examined the effect of hexagonal angle, loading direction and packing system on the crushing behavior, energy absorption, failure mechanism and failure mode of composite hexagonal rings. Deruntz and Hodge [19] performed a simple rigid plastic analysis on the lateral compression of a circular tube and obtained load–deformation curve of the tubes crushed between two rigid parallel plates. They quantitatively discussed the effects of direct stress and shear on the yield condition.

The present article investigates the flattening process on metal columns with square and rectangular cross-sections subjected to lateral compression load by theoretical and experimental methods. Some theoretical relations are derived to predict the lateral force, absorbed energy and specific absorbed energy by the specimens, based on the energy method. Also, some lateral compression tests are performed on the aluminum and brazen columns with square and rectangular cross-sections to verify the theoretical formulas and to study the effects of geometrical characteristics and material types of the columns on their energy absorption capability.

2. Theory

By exerting lateral compression load on a rectangular column vertically, the lateral load applies on the lower and upper column edges. At the commencement of loading, both the left and right edges are axially compressed, in the elastic zone. Then, plastic hinge lines form at the mid-height of the vertical arms. By increasing the lateral compression, the

vertical edges deformed outward while the horizontal edges bend inward. Simultaneously, four hinge lines form at the four corners of the column cross-section, effectively. Finally, the column changes to a double layers plate. Fig. 1 shows a rectangular column during the lateral compression test that is called flattening process.

In the present theoretical analysis, it is assumed that square and rectangular columns are compressed symmetrically, during the flattening process. Fig. 2 indicates the theoretical model of columns deformation during the lateral compression. It is assumed that the plastic hinge lines form at the mid-height of the vertical arms (points C and H). Curvature of the horizontal edges is neglected, because bending of the horizontal arms dissipates a small amount of energy, comparing with the other deformation mechanisms. According to the introduced model, it is considered that the four corner angles (at points A, B, D and G) increase continuously during the plastic deformation.

In the theoretical analysis, deformation process divides into two different stages and based on the energy method, the absorbed energy by different deformation mechanisms is calculated. First stage investigates the plastic deformation and the second stage estimates the elastic zone.

2.1. *First stage: plastic deformation*

Absorbed energy by a plate during bending around a plastic hinge line is obtained as the following:

$$E = \int M_0 L d\theta = M_0 L \theta \tag{1}$$

Wierzbicki and Abramowicz [20] used the above relation to predict the axial load of a square column during the folding deformation and introduced the super-folding element. In the above equation, L and θ are the length of the plastic hinge line and the rotation angle of side panels around the hinge line, respectively. M_0 is the perfectly plastic bending moment per unit of length and is calculated as

$$M_0 = \frac{\sigma_0 t^2}{4} \tag{2}$$

where, t is the column wall thickness and σ_0 is the flow stress of the column material. Flow stress is calculated as the following [21]:

$$\sigma_0 = \sqrt{\frac{(\sigma_y \sigma_u)}{1+n}} \tag{3}$$

In the above equation, σ_y, σ_u and n indicate the yield stress, ultimate stress and strain hardening exponent, respectively which are obtained from the quasi-static tension test on a standard dumbbell shape specimen. In the present theory, the column material is assumed rigid-perfectly plastic and therefore, σ_0 and M_0 are constant. Thus, the dissipated energy due to the plastic deformation in the hinge line of each vertical arm (points C and H) is computed as

$$E_1 = M_0 L \gamma \tag{4}$$

In the above equation, L indicates the column length and γ is the rotation angle around the hinge line of each vertical arm and varies from 0 to π.

Four corner angles (points A, B, D and G) dissipate the energy due to the angle increment. Each corner angle varies from $\pi/2$ to π, so, the angle variation is between 0 and $\pi/2$. Therefore, the absorbed energy by each corner plastic hinge line is obtained as

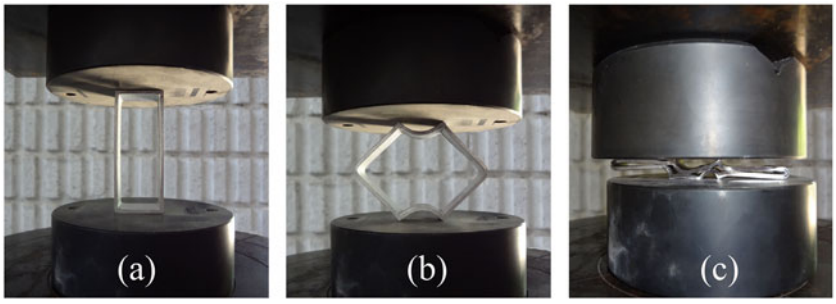

Fig. 1 – An aluminum column during the test.

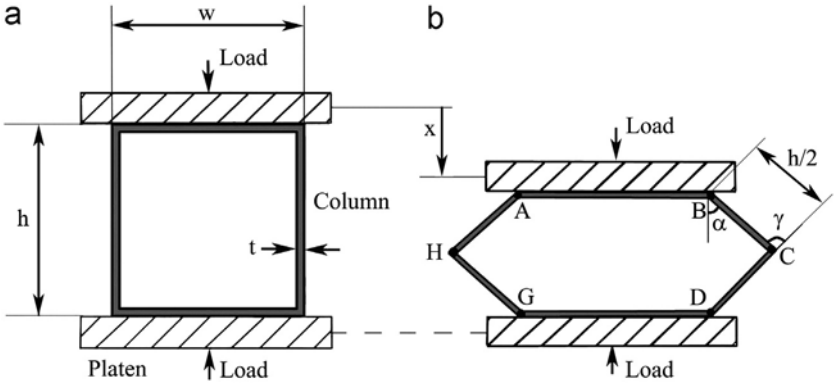

Fig. 2 – Theoretical model of plastic deformation of rectangular metal column during the flattening process between two rigid plates.

$$E_2 = M_0 L\alpha \tag{5}$$

Angle α is shown in Fig. 2. There is the following relation between α and γ:

$$\gamma = 2\alpha \tag{6}$$

Therefore, the total absorbed energy by a rectangular column during the flattening process is calculated as the following:

$$E_{int} = 2E_1 + 4E_2 = 8M_0 L\alpha \tag{7}$$

In the above equation, α varies with respect to the instantaneous lateral displacement (x) as the following relation:

$$\alpha = \cos^{-1}\left(\frac{h-x}{h}\right) \tag{8}$$

where h is the length of the vertical edge of the column, as shown in Fig. 2. Substituting (8) in (7) results in

$$E_{int} = 2\sigma_0 L t^2 \cos^{-1}\left(\frac{h-x}{h}\right) \tag{9}$$

The dissipated energy in the elastic part is reversible and its magnitude is small, comparing with the dissipated energy in the plastic part. Therefore, the absorbed energy during the elastic deformation is neglected. Thus, Eq. (9) predicts theoretical diagram of the dissipated energy versus the lateral displacement all over the deformation process of a rectangular column.

The applied external work by the lateral load on a rectangular column during the lateral compression is calculated as

$$W_{ext} = P_p x \tag{10}$$

Based on the principle of the energy conservation and energy method, the applied external work by the lateral load (Eq. (9)) is equated to the internal dissipated energy by the column (Eq. (10)), $W_{ext}=E_{int}$. Therefore

$$P_p = \frac{2\sigma_0 L t^2 \cos^{-1}((h-x)/h)}{x} \tag{11}$$

P_p is the instantaneous lateral load in the plastic part of the flattening process. The above equation predicts the plastic part of the lateral load–lateral displacement diagram during the lateral compression of a rectangular column. Eq. (11) shows that at commencement of loading, $x=0$ and P_p inclines to a non-limited value. Therefore, Eq. (11) can nly predict the plastic part of the load–displacement curve. Therefore, the mentioned equation estimates the lateral load, when $x \geq x_{cr}$ and x_{cr} is the maximum lateral elastic displacement.

Mass of a column is obtained as

$$m = 2\rho L t(h + w - 2t) \tag{12}$$

where ρ is the density of the column material. w and the other geometrical dimensions of the column are shown in Fig. 2. The specific absorbed energy (SAE) or absorbed energy per unit of the column mass is derived as

$$SAE = \frac{E_{int}}{m} = \frac{\sigma_0 t \cos^{-1}((h-x)/h)}{\rho(h + w - 2t)} \tag{13}$$

2.2. Second stage: elastic deformation

At commencement of loading, the left and right edges of the column cross-section are compressed during the elastic deformation and the process continues until the lateral load reaches to the critical buckling load of two vertical edges. It shows end point of the elastic zone. Two end points of each vertical edge can rotate; therefore, each vertical edge is assumed as a two end pin-connected column subjected to an axial load. The critical buckling load of each vertical arm is obtained by using Euler's formula:

$$P_{cr} = \frac{\pi^2 EI}{L_e^2} \tag{14}$$

In which, E is the modulus of elasticity, L_e is the effective length and is equal to length of each vertical edge of the column cross-section, h. Also, I is the second moment of area and is equal to $Lt^3/12$. So, the critical buckling load of the column or the maximum lateral load in the elastic zone is calculated as

$$P_{cr} = \frac{\pi^2 E L t^3}{6h^2} \tag{15}$$

In the elastic part, the load is assumed proportional to the lateral displacement. To derive a theoretical relation for predicting the elastic part of the load–displacement curve, coordinates of two points of (0, 0) and (x_{cr}, P_{cr}) are needed. x_{cr} is the corresponding displacement of the critical buckling load P_{cr}.

The end point of the elastic zone is the cross over point of the elastic and plastic curves; therefore, root of equation $P_p = P_{cr}$ determines the critical lateral displacement as the following:

$$\frac{x_{cr}}{h} = 1 - \cos\left(\frac{P_{cr} x_{cr}}{8M_0 L}\right) \tag{16}$$

According to the series expansion, it results in

$$\cos\left(\frac{P_{cr} x_{cr}}{8M_0 L}\right) \approx 1 - \frac{((P_{cr} x_{cr})/(8M_0 L))^2}{2!} \tag{17}$$

x_{cr} is a small quantity. Therefore, in the above equation, more than the second order terms were neglected. Substituting (17) in (16) results in

$$x_{cr} = \frac{128 M_0^2 L^2}{h P_{cr}^2} = \frac{288\sigma_0^2 h^3}{\pi^4 E^2 t^2} \tag{18}$$

Substituting the critical displacement from (18) in (11) results in the following relation to predict the minimum value of the required lateral load of flattening creation in a rectangular column:

$$P_{max} = \frac{2\sigma_0 L t^2 \cos^{-1}((h-x_{cr})/h)}{x_{cr}} \tag{19}$$

The following relation is derived to estimate the elastic part of the load–displacement diagram:

$$P_e = \frac{P_{cr}}{x_{cr}} x = \frac{\pi^6 K^3 L t^5}{1728 h^5 \sigma_0^2} x \tag{20}$$

Finally, the lateral load versus the lateral displacement during the flattening process in the rectangular and square

columns is derived as

$$P=\begin{cases}\dfrac{\pi^6E^3Lt^5}{1728h^5\sigma_0^2}x, & x\le x_{cr}\\ \dfrac{2\sigma_0Lt^2\ \cos^{-1}((h-x)/h)}{x}, & x_{cr}\le x\le h\end{cases} \tag{21}$$

3. Experiment

Lateral compression tests were carried out on brazen and aluminum specimens with square and rectangular cross-sections between two rigid plates to verify the theoretical analysis. All the flattening tests were performed by a DMG machine, model 7166 at a constant crosshead speed of 10 mm/min in quasi-static condition. In all the experiments, load–deformation curves were obtained by machine chart recorder. The tests were performed on four groups of brazen columns and 11 groups of aluminum specimens. All of the brazen specimens were prepared with square cross-section. Four groups of the aluminum specimens were prepared with square cross-section and the other aluminum specimens were prepared with rectangular cross-section. Some similar specimens of the aluminum columns with rectangular cross-section were prepared and compressed along the longer and the shorter edges of the cross-section to compare the results. Fig. 3 shows two aluminum rectangular specimens with the same dimensions that were compressed along different sides, before and after the tests.

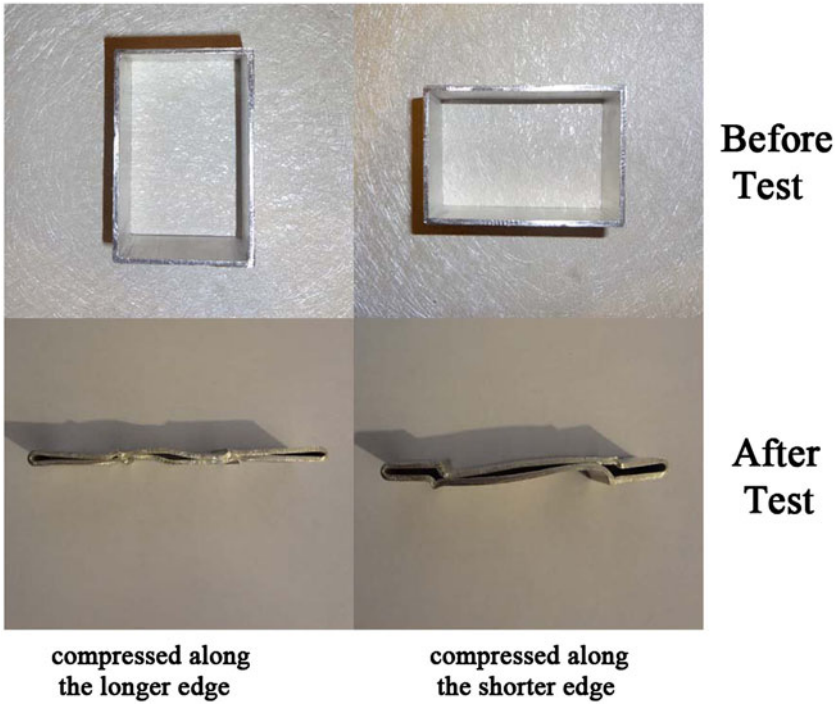

Fig. 3 – Two same rectangular specimens that compressed along two different directions, before and after tests.

Table 1 – Geometrical characteristics of the specimens.

Specimen code	t (mm)	Cross-section		Material	L (mm)	m (g)
		h (mm)	w (mm)			
E-1	1.0	35	35	Brass alloy	43.2	50.7
E-2	1.0	35	35	Brass alloy	61.1	71.5
E-3	1.0	40	40	Brass alloy	37.8	52.9
E-4	1.0	40	40	Brass alloy	47.1	65.9
A-01	1.9	35	35	Aluminum alloy	19.7	11.75
A-02	1.8	45	45	Aluminum alloy	19.9	14.22
A-03	1.8	45	45	Aluminum alloy	45	32.47
A-04	1.8	45	45	Aluminum alloy	90	64.94
A-05	1.7	55	35	Aluminum alloy	20.5	13.36
A-06	1.7	35	55	Aluminum alloy	22	14.19
A-07	1.7	55	35	Aluminum alloy	36.4	23.78
A-08	1.7	55	35	Aluminum alloy	69.9	52.72
A-09	2.0	25	64	Aluminum alloy	20.7	17.5
A-10	2.0	64	25	Aluminum alloy	21	17.6
A-11	2.0	64	25	Aluminum alloy	40.8	34.4

Table 1 gives characteristics of the specimens. In the table, m, t and L are the mass, wall thickness and length of the specimens, respectively. The specimens with the different cross-sections and dimensions were studied to investigate the effects of geometrical parameters on the energy absorption capability of the structure. For each case, three similar specimens were prepared to prove repeatability of the experiments. Table 2 gives material properties of the tested specimens which were obtained by quasi-static tension tests on a standard dumbbell shape specimen of each column material, according to ASTM E8M.

4. Results and discussion

Based on energy method, some theoretical relations were derived to predict the absorbed energy during the flattening process of rectangular columns. Some experiments were performed on the brazen and aluminum columns with square and rectangular cross-sections. Energy absorption, specific absorbed energy and lateral load were measured in each test to verify the derived equations and also to study the effects of different geometrical characteristics of the specimens on the absorbed energy by the columns.

4.1. *Verification of theoretical load–displacement equation*

Eq. (21) predicts load–displacement diagram of square and rectangular columns subjected to lateral compression load between two rigid plates in quasi-static condition. The first expression of the equation predicts the elastic part of the load–displacement diagram and the second expression predicts the plastic part. According to the mentioned relation, the lateral load of a rectangular column during the flattening process is a function of lateral displacement (x), material properties and the column dimensions. Figs. 4 and 5 compare the theoretical and experimental diagrams of lateral load versus lateral displacement of two different aluminum columns and Figs. 6 and 7 compare the corresponding curves of the brazen specimens. In some parts of the load–displacement diagrams, Eq. (21) estimates the lateral load higher than the experimental measurements. It is because of neglecting the created curvature in the horizontal edges of the column cross-section. In the last part of the load–displacement diagrams, the lateral load increases intensively while, the lateral displacement increases slightly. The reason is that in the experiments, in this stage, two horizontal edges reach to each other and their bending begins outward. In the present theory, the effects of bending of horizontal edges on the absorbed energy by columns were

Table 2 – Properties of the columns materials.

Material	Cross-section (mm × mm)	Yield stress (MPa)	Ultimate stress (MPa)	Strain hardening exponent	Flow stress (MPa)	Elastic modulus (GPa)	Density (kg/m^3)
Brass alloy	35 × 35	307	447.92	0.45	307.95	105	8616.94
Brass alloy	40 × 40	260	396.28	0.49	262.96	105	8969.55
Aluminum alloy	35 × 35	173	237	0.17	186.6	75	2371.34
Aluminum alloy	45 × 45	205	246.76	0.13	211.55	70	2312.48
Aluminum alloy	55 × 35	128	158.08	0.10	135.38	70	2282.29
Aluminum alloy	64 × 25	205	246.76	0.13	211.55	75	2449.35

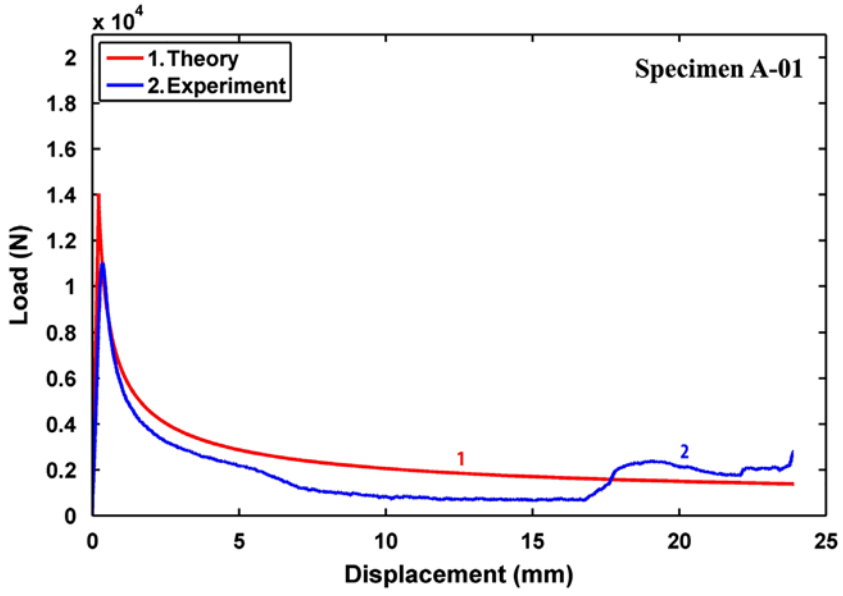

Fig. 4 – Theoretical and experimental load–displacement diagrams of specimen A-01.

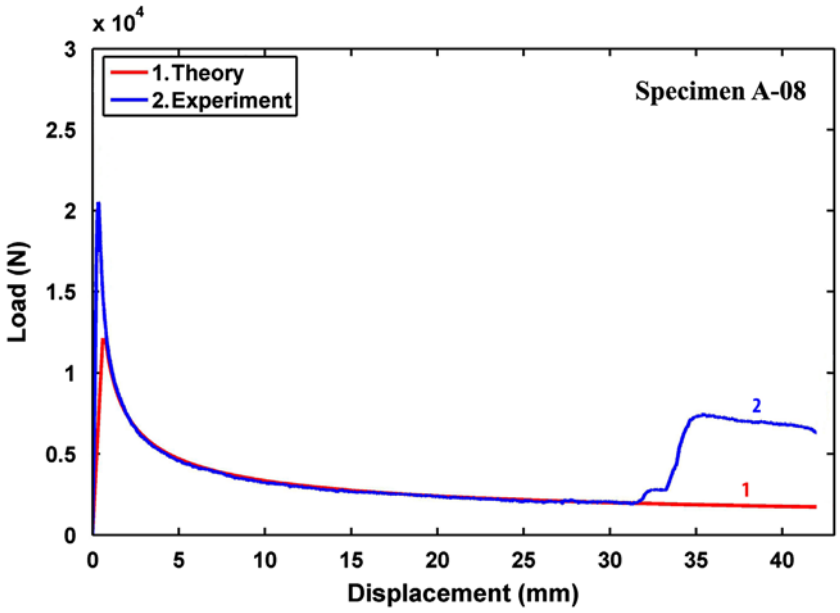

Fig. 5 – Theoretical and experimental load–displacement diagrams of specimen A-08.

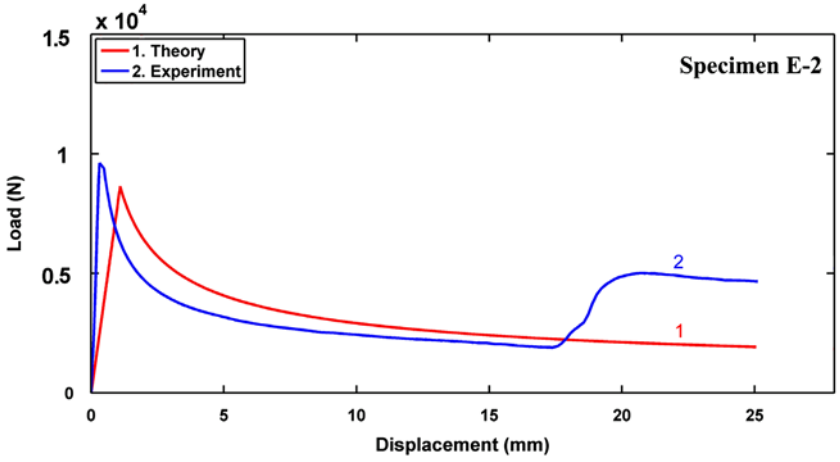

Fig. 6 – Theoretical and experimental load–displacement diagrams of specimen E-2.

neglected. Reviewing the theoretical and experimental comparisons shows that the theoretical formula gives a good approximation of the load–displacement curve.

4.2. *Verification of theoretical dissipated energy–displacement equation*

Eq. (9) computes the absorbed energy by square and rectangular columns during the flattening process. According to the equation, the dissipated energy by a rectangular column is dependent on the material properties and geometrical characteristics of the column. Dissipated energy by a certain specimen varies when the rotation angle of the side panels increases and consequently, when the lateral displacement increases. Figs. 8–11 show the absorbed energy–displacement curves of four different specimens and compare each theoretical curve with the corresponding experimental diagram. Theoretical and experimental results show that the absorbed energy by empty square and rectangular columns nonlinearly increases versus the lateral displacement during the flattening process. In the last part of the absorbed energy–displacement diagram, the experimental curves have a considerable difference with the theoretical ones. However, the present theoretical relation predicts the absorbed energy versus the lateral displacement with a very good correlation in the most parts, comparing with the experiments. Also, comparison of slopes of theoretical and experimental curves in different zones concludes that the general form of the obtained mathematical function for predicting the absorbed energy by a rectangular column is correct.

4.3. *Verification of theoretical SAE equation*

Specific absorbed energy (SAE) or energy absorption per unit of structure mass is the most important parameter in design and manufacturing of an energy absorber. When the specific absorbed energy by the structure increases, the energy absorber efficiency increases, too.

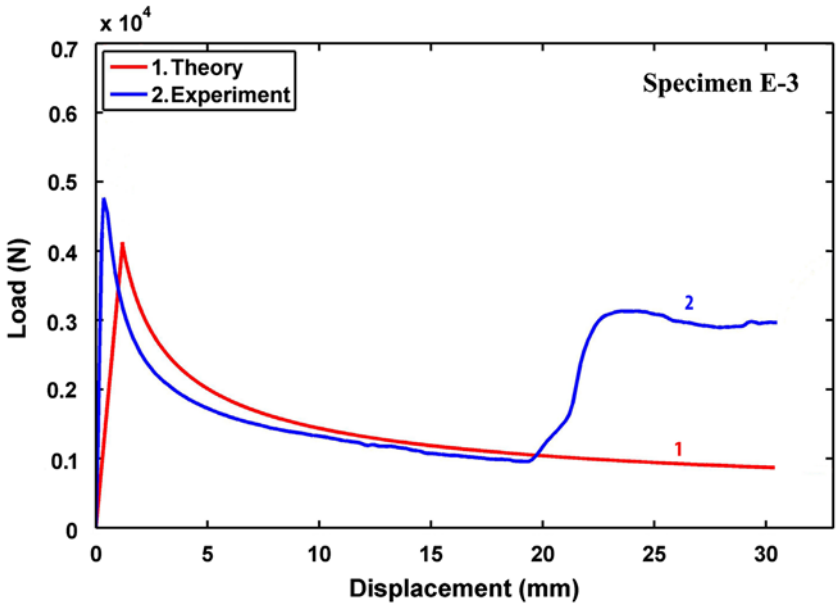

Fig. 7 – Theoretical and experimental load–displacement diagrams of specimen E-3.

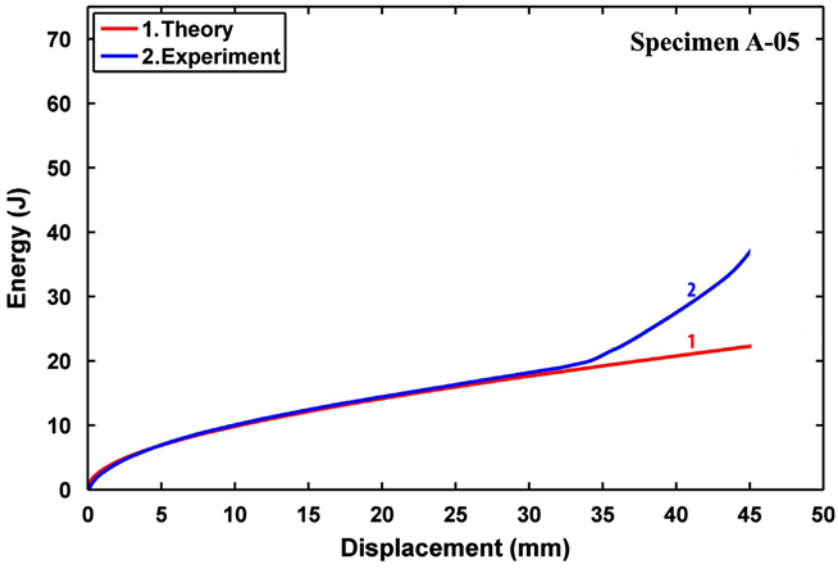

Fig. 8 – Theoretical and experimental absorbed energy–displacement diagrams of specimen A-05.

Eq. (13) estimates the SAE by metal rectangular columns under lateral compression load between two rigid plates as a function of material properties, geometrical characteristics and lateral displacement of the columns. Figs. 12–15 show predicted diagrams of the SAE by theoretical Eq. (13) versus lateral displacement and compare it with the corresponding experimental curves.

In specific absorbed energy–displacement diagrams, the theoretical curves are usually lower than the experimental ones. It is because in the theoretical analysis, two different deformation modes consist of plastic hinge lines formation in midpoints of the vertical edges and two end points of the horizontal edges were considered and bending of the horizontal arms was neglected.

4.4. *Verification of theoretical maximum lateral load and elastic load*

Eq. (19) predicts the minimum value of the required lateral load for flattening a rectangular metal column between two rigid plates (P_{max}). It is the maximum lateral force of the load–displacement curve during the flattening process. Table 3 compares the theoretical and experimental values of the maximum lateral load of each specimen. Also, the error percentages of theoretical predictions are given. According to the table, the error percentage of 53% of the specimens is less than 16% and the error percentage of 80% of the specimens is less than 29%. Thus, Eq. (19) gives a good approximation of the experimental results. The theoretical results show

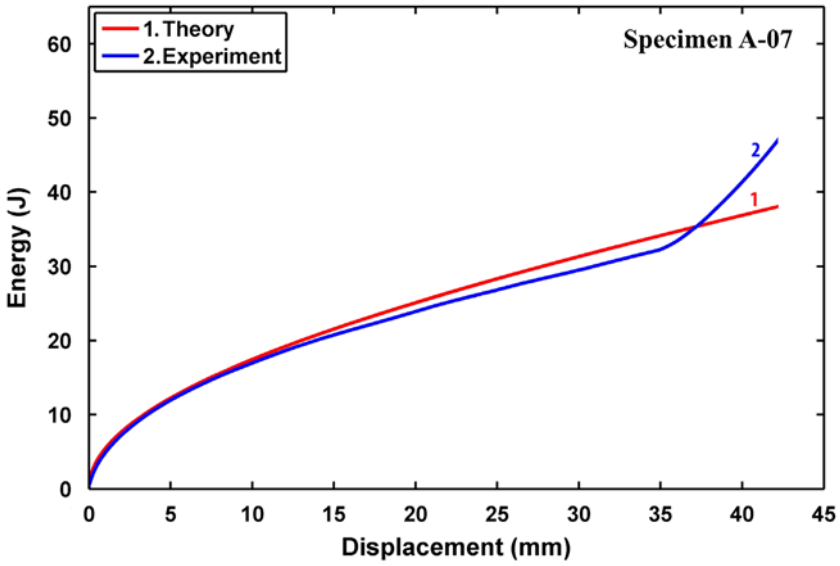

Fig. 9 – Theoretical and experimental absorbed energy–displacement diagrams of specimen A-07.

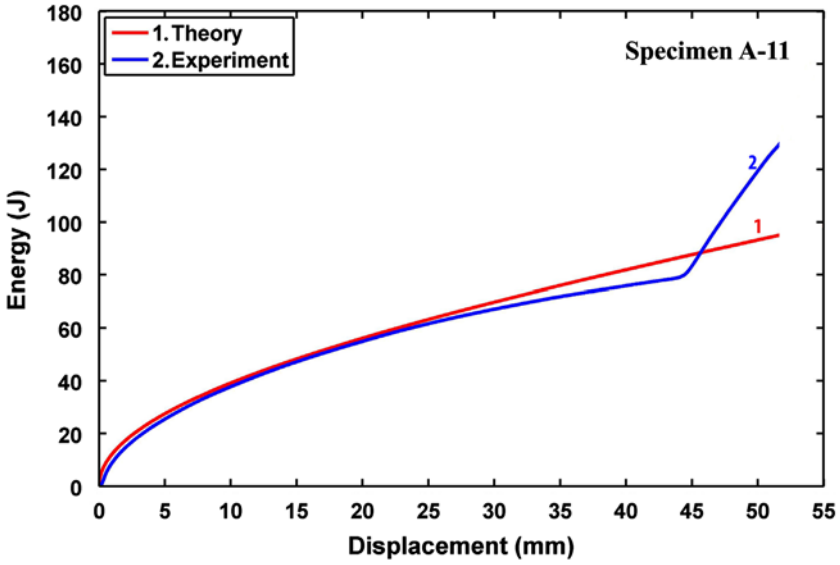

Fig. 10 – Theoretical and experimental absorbed energy–displacement diagrams of specimen A-11.

that Eq. (19) estimates the maximum lateral load of rectangular columns A-06 and A-09, which were compressed along the shorter edge of their cross-section with a considerable error percentage, but, for the other specimens the theoretical predictions of the maximum lateral load have a satisfactory accuracy, comparing with the experiments.

In the theoretical analysis, Eq. (20) was derived to estimate the elastic part of the lateral load–displacement diagram of the rectangular columns during the flattening process, theoretically and for this purpose, Euler's formula was used to calculate the critical buckling load of each vertical arm as the start point of the plastic deformation. Eq. (20) was calculated by assuming each vertical edge of the column as two ends pin-connected column and it was assumed that when the lateral load reaches to the critical buckling load of two vertical edges, the elastic zone is terminated. Figs. 4–7 show that slope of each theoretical load–displacement curve is approximately near to slope of the corresponding experimental curve. So, theoretical Eq. (20) predicts the elastic part of the load–displacement curve with a reasonable agreement and therefore, the initial assumptions during derivation of theoretical Eq. (20) and also, theoretical model of buckling in the vertical edges of columns are coincided with the mechanical behavior of the specimens.

4.5. *Effect of column length*

Fig. 16 shows the experimental diagram of lateral load per unit of column length (load/length) of two aluminum specimens with the same material, wall thickness and cross-section dimensions and different lengths versus the lateral displacement. Also, Fig. 17 indicates the experimental diagram of the

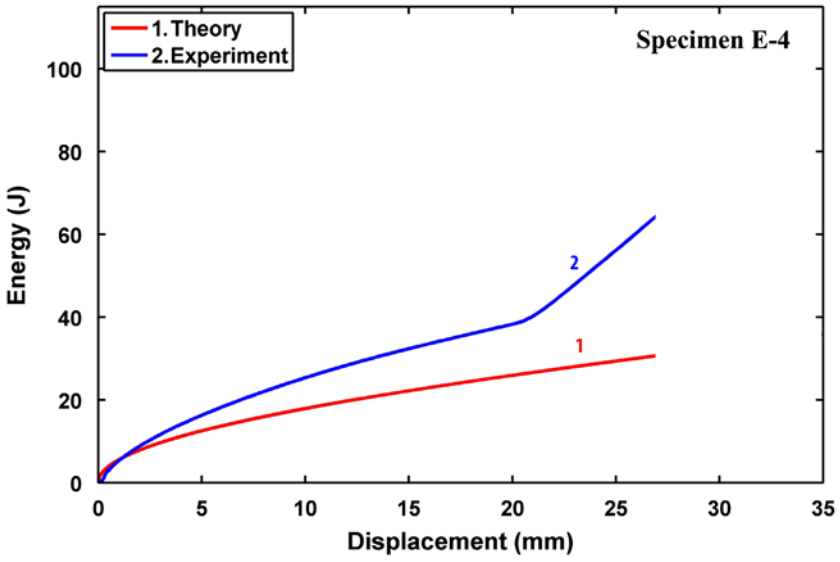

Fig. 11 – Theoretical and experimental absorbed energy–displacement diagrams of specimen E-4.

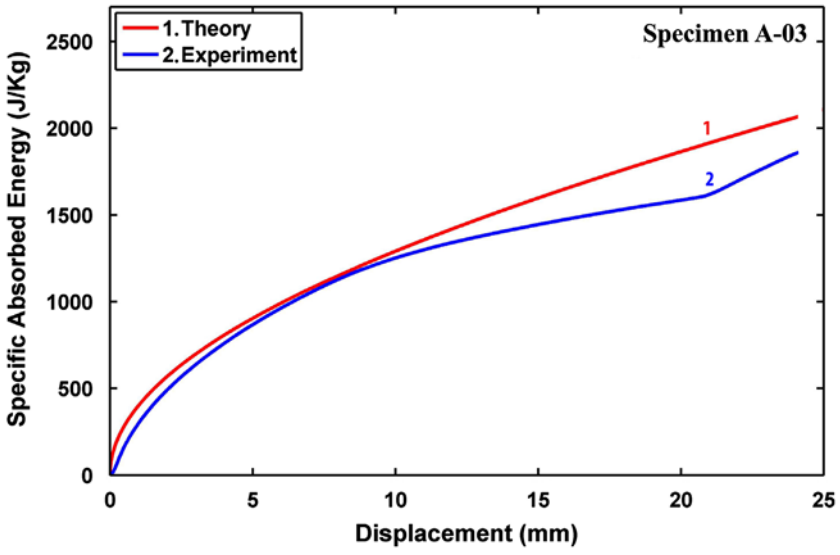

Fig. 12 – Theoretical and experimental specific absorbed energy–displacement diagrams of specimen A-03.

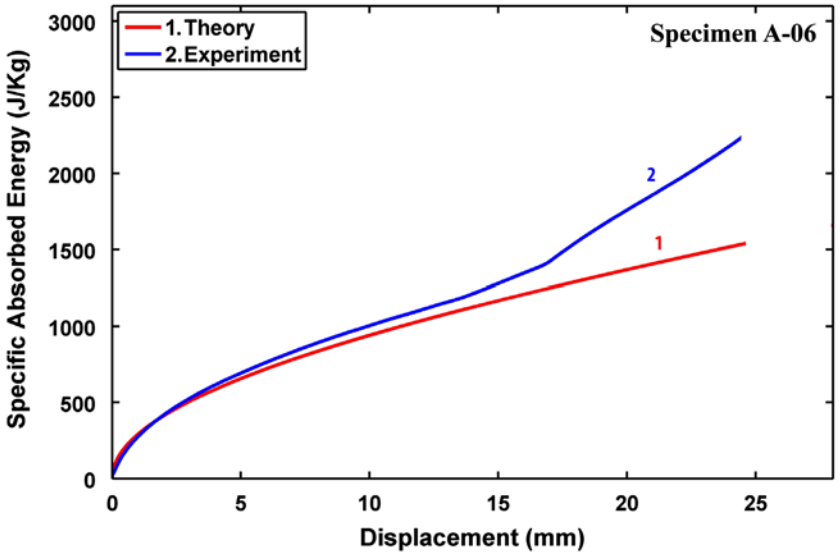

Fig. 13 – Theoretical and experimental specific absorbed energy–displacement diagrams of specimen A-06.

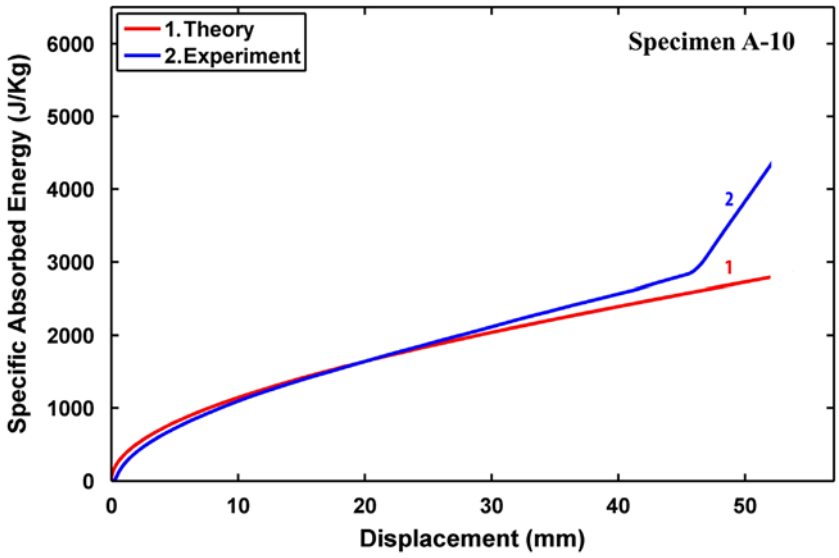

Fig. 14 – Theoretical and experimental specific absorbed energy–displacement diagrams of specimen A-10.

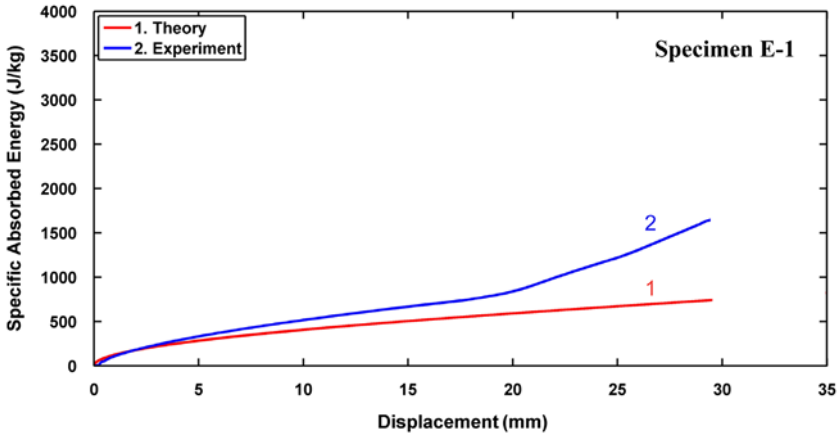

Fig. 15 – Theoretical and experimental specific absorbed energy–displacement diagrams of specimen E-1.

Table 3 – Comparison between the theoretical predictions and experimental results of maximum lateral load.

Specimen code	P_{max} (kN)		Error percentage (%)
	Theory	Experiment	
E-1	6.27	6.77	7.38
E-2	8.85	9.61	7.91
E-3	4.10	4.77	14.05
E-4	5.09	6.03	15.59
A-01	13.53	11.02	22.78
A-02	6.61	5.26	25.66
A-03	14.94	13.82	8.10
A-04	29.88	25.80	15.81
A-05	3.83	3.96	3.28
A-06	10.29	5.28	94.89
A-07	6.79	6.66	1.95
A-08	13.15	20.54	35.99
A-9	33.03	13.40	146.49
A-10	5.14	6.74	23.74
A-11	9.99	14.00	28.64

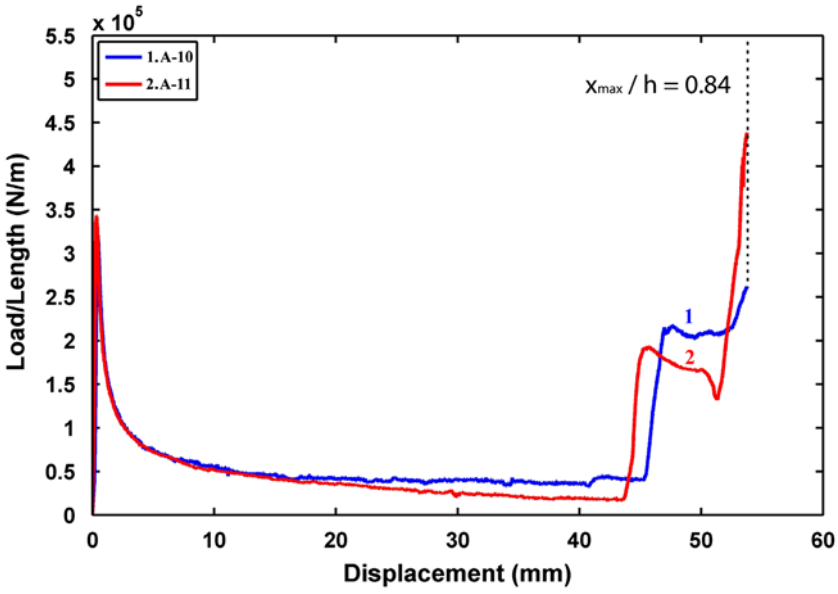

Fig. 16 – Diagram of lateral load/length versus displacement of two aluminum specimens with the same cross-section and different lengths.

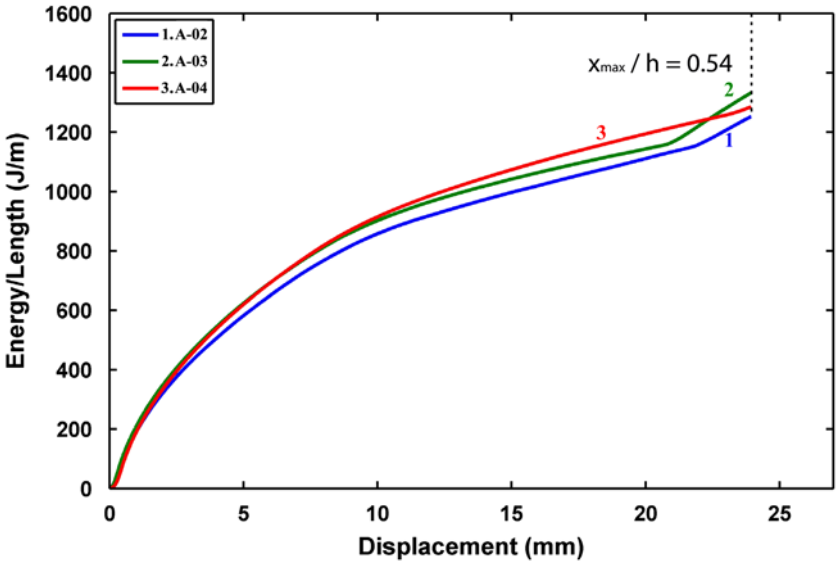

Fig. 17 – The experimental diagram of the absorbed energy/length versus displacement of three aluminum specimens with the same cross-section and different lengths.

absorbed energy per unit of column length (energy/length) of three specimens with different lengths but the same other corresponding dimensions and materials. Experimental results show that the absorbed energy by a column during flattening process has a direct relationship with the specimen length. On the other hand, when the column length increases, the lateral load and the absorbed energy increase, linearly. Also, Eqs. (9) and (21) theoretically prove that the lateral load and the absorbed energy by a flattened column increase proportional to the column length. Therefore, the theoretical formulas and the experimental measurements show the same results for the effects of column length.

4.6. *Effect of column cross-section dimensions*

Fig. 18 shows the specific absorbed energy by square and rectangular columns with different cross-section dimensions. The specific absorbed energy by all the mentioned specimens in Fig. 18 was calculated up to a same ratio of x/h. In the figure, brazen specimens E-2 and E-4 and aluminum columns A-01 and A-04 were prepared with square cross-section and different dimensions. Each edge length of the square cross-section of specimens E-2 and A-01 is longer than the corresponding dimensions of E-4 and A-04, respectively. The experimental results show that in both the brazen and

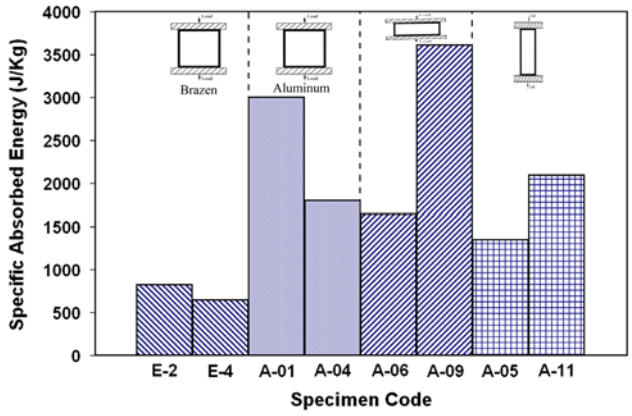

Fig. 18 – Comparison between the specific absorbed energy by different specimens.

aluminum columns with square cross-section, when the edge length increases, the specific absorbed energy by the column decreases. Therefore, decreasing the edge length of flattened square columns makes a better energy absorber.

4.7. *Effect of column wall thickness*

Fig. 19 shows the total specific absorbed energy versus the column wall thickness, based on theoretical Eq. (13). The curve shows that when the wall thickness of the column increases, the total SAE by the specimen increases, nonlinearly. Therefore, rectangular columns with the thicker wall are the better energy absorbers during the flattening process.

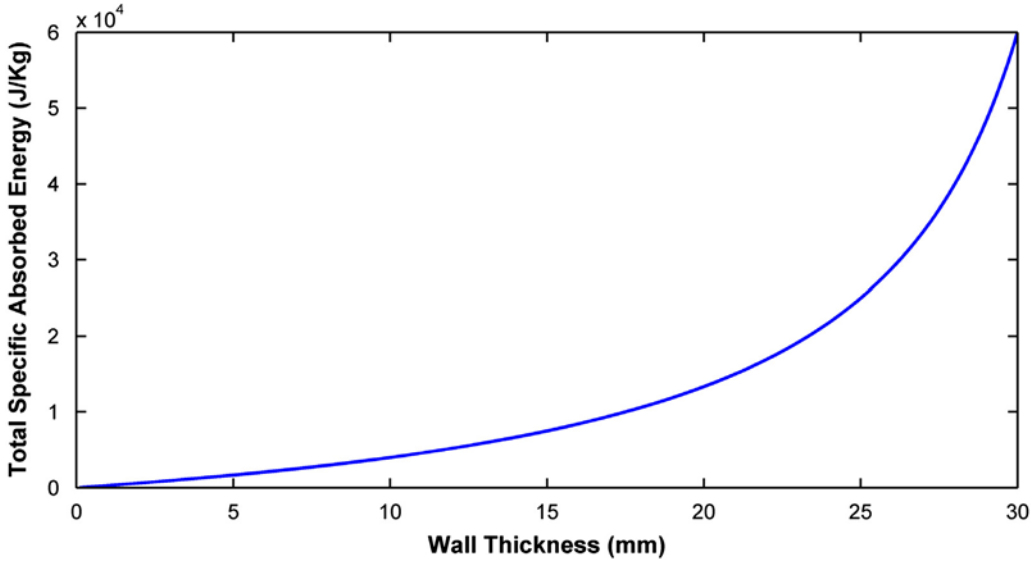

Fig. 19 – Theoretical diagram of total specific absorbed energy versus the column wall thickness.

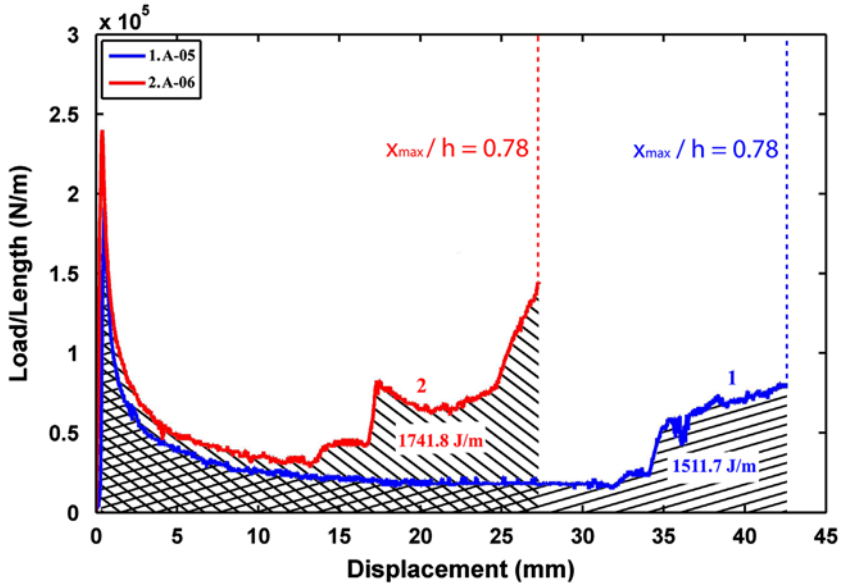

Fig. 20 – Comparison between the load/length–displacement diagrams of specimens A-05 and A-06.

4.8. *Effect of column material*

In Fig. 18, specimens E-2 and A-01 have the same cross-section dimensions but, they are made from brass and aluminum, respectively. A comparison of the experimental results of aluminum and brazen specimens indicates that aluminum columns subjected to the lateral compression load have the higher energy absorption capability than the brazen ones. It is because the aluminum density is less than the brass density, and the flow stress of the aluminum is less than the brass, too. Therefore, the flow stress/density ratio of the aluminum is larger than the corresponding quantity of the brass. Therefore, the aluminum columns are the more efficient energy absorbers, comparing with the brazen columns during the flattening process. Also, Eq. (13) theoretically proves that the flattened columns with the high ratio of the flow stress/density are the better energy absorbers. Therefore, the theoretical analysis and the experimental measurements show a good agreement and the same results.

4.9. *Comparison of the flattening process of the same rectangular columns along two different directions*

In Fig. 18, specimens A-09 and A-11 are the same. But, A-09 was compressed along the shorter edge of its cross-section and A-11 was compressed along the longer edge. The figure shows that A-09 has more energy absorption capacity, comparing with the specimen A-11. Fig. 20 represents diagram of the load/length–lateral displacement of the same dimensional aluminum columns A-05 and A-06 with rectangular cross-section and Fig. 21 illustrates corresponding diagram of the same characteristic aluminum specimens A-09 and A-10. Rectangular specimens A-06 and A-09 are compressed along their shorter edges and the specimens A-05 and A-10 are

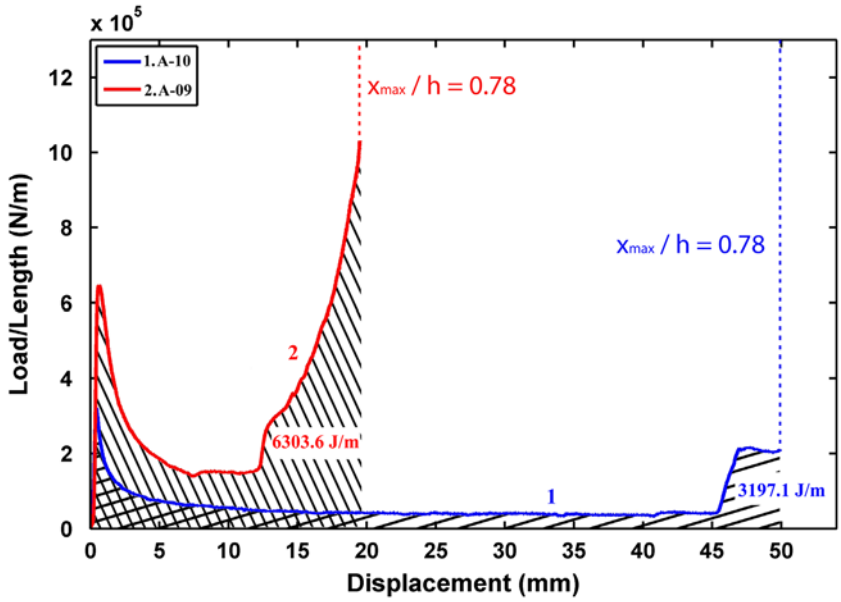

Fig. 21 – Comparison between the load/length–displacement diagrams of specimens A-09 and A-10.

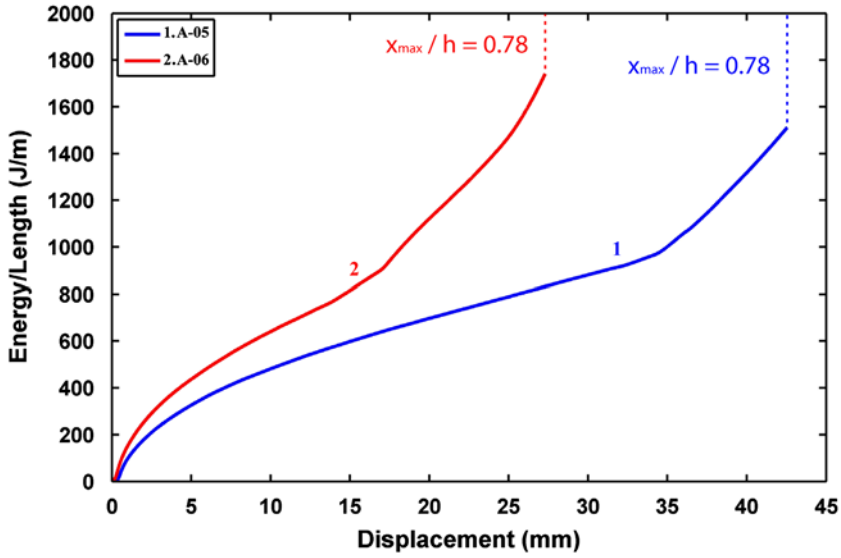

Fig. 22 – Comparison between the energy/length–displacement diagrams of specimens A-05 and A-06.

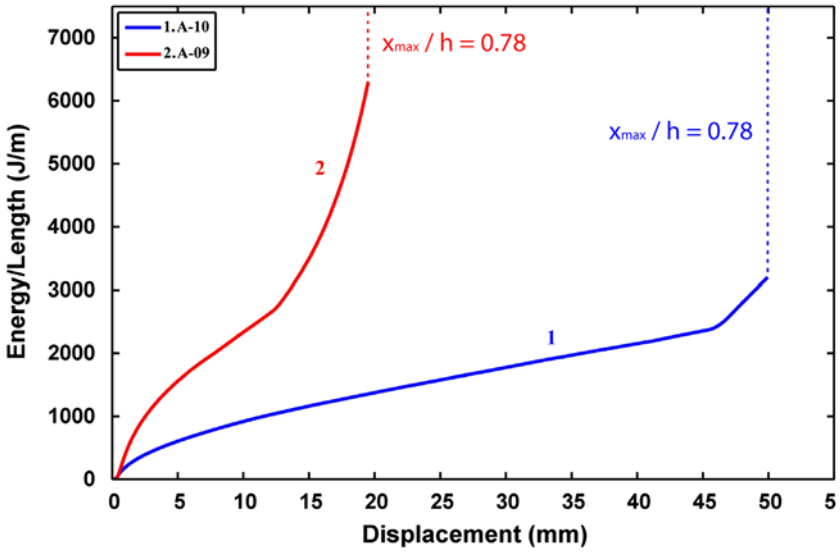

Fig. 23 – Comparison between the energy/length–displacement diagrams of specimens A-09 and A-10.

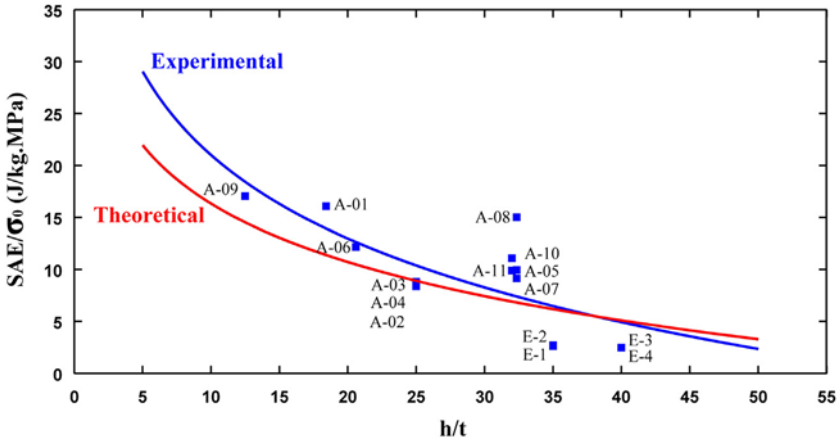

Fig. 24 – Experimental and theoretical diagrams of the SAE/flow stress ratio versus the h/t ratio.

compressed along their longer edges. The area under the load/length–displacement diagram of each specimen shows the absorbed energy per unit of column length. Figs. 20 and 21 show that compression of a rectangular column along the shorter edge of cross-section dissipates more energy than compression of the same specimen along the longer edge. Figs. 22 and 23 compare diagrams of the energy/length ratio versus lateral displacement of the mentioned specimens. According to the graphs, at a certain lateral displacement, the lateral load and the absorbed energy by the rectangular column that is compressed along the shorter edge are more than the corresponding quantities of the same column that is flattened along the longer edge. Eq. (9) affirms the same results, theoretically. In this analytical equation, at a certain displacement, by increasing the h, the absorbed energy decreases.

4.10. *Effect of h/t ratio*

Fig. 24 represents ratio of the specific absorbed energy/flow stress of the different specimens versus the h/t ratio. Both the theoretical and experimental curves are sketched in the figure. The experimental curve was obtained by curve fitting the experimental measurements that are shown by the square markers. Also, by substituting the columns characteristics in theoretical Eq. (13), the corresponding theoretical curve was sketched. A reasonable correlation between the curves affirms verity of the present theory. Also, the figure shows that when the h/t ratio increases the specific absorbed energy/flow stress of the column decreases, nonlinearly. For example, the experimental measurements result that the specimens A-01 and A-05 with the same horizontal edges length (w) but, different vertical edges lengths (h) and thicknesses (t) have different ratios of the specific absorbed energy/flow stress equal to 16.07 and 9.95 J/kg MPa, respectively. Therefore, the SAE/flow stress of the specimen A-01 is about 1.62 times of the corresponding value of the specimen A-05, while, the h/t ratio of the specimen A-05 is about 1.76 times of the corresponding ratio of the specimen A-01.

4.11. *Effect of friction between plates and the specimen*

Friction between plates and the specimen causes tension in the horizontal edges when the load begins to act at the

corners. Previously, Gupta and Khullar showed that tension of the horizontal edges increases the effective stiffness of the arms [2]. By increasing the effective stiffness of the arms, more energy is required to bend them. Therefore, the higher value of friction coefficient between the plates and the horizontal arms results in the higher energy absorption by the column. So, the absorbed energy by the column has a direct relation with the friction factor between the column and the plates. However, in the present work, the specimens were lubricated before the tests, and therefore, in the theoretical analysis, the effects of friction on the lateral load were neglected, comparing with the absorbed energy by the plastic deformations.

5. Conclusion

This paper presents theoretical and experimental analyses on the metal rectangular and square columns during the flattening process under lateral compression load. Based on the energy method, some theoretical formulas were derived to predict the instantaneous lateral load, the absorbed energy and the specific absorbed energy by the columns as functions of lateral displacement, geometrical characteristics, and material properties of the columns. Comparison of the theoretical predictions and experimental results shows that although, Eq. (19) estimates the maximum lateral load of rectangular columns which were compressed along the shorter edge of their cross-section such as specimens A-06 and A-09, with a considerable error percentage, for the other cases, a good correlation was shown between the analytical and experimental results. Therefore, the general form of the presented theoretical formulas is correct. Also, based on the lateral compression tests on the aluminum and brazen columns with square and rectangular cross-sections it is concluded that the lateral load and the absorbed energy by a flattened column increase proportional to the column length. Also, the specific absorbed energy nonlinearly increases when the column wall thickness increases. Experiments show that the lateral load and the absorbed energy by the rectangular column that is compressed along the shorter edge are more than the corresponding quantities of the same column that is flattened along the longer edge. Also, the aluminum columns subjected to the lateral compression load have the higher energy absorption capability, comparing with the brazen ones. Experimental and theoretical results illustrate that the specific absorbed energy by a column has an inverse relation versus the h/t ratio.

REFERENCES

[1] A.G. Olabi, E. Morris, M.S.J. Hashmi, M.D. Gilchrist, Optimised design of nested oblong tube energy absorbers under lateral impact loading, International Journal of Impact Engineering 35 (2008) 10–26.

[2] N.K. Gupta, A. Khullar, Collapse load analysis of square and rectangular tubes subjected to transverse in-plane loading, Thin-Walled Structures 21 (1995) 345–358.

[3] N.K. Gupta, H. Abbas, Lateral collapse of composite cylindrical tubes between flat platens, International Journal of Impact Engineering 24 (2000) 329–346.

[4] N.K. Gupta, G.S. Sekhon, P.K. Gupta, A study of lateral collapse of square and rectangular metallic tubes, Thin-Walled Structures 39 (2001) 745–772.

[5] M. Zeinoddini, G.A.R Parke, J.E. Harding, Axially pre-loaded steel tubes subjected to lateral impacts: an experimental study, International Journal of Impact Engineering 27 (2002) 669–690.

[6] S.A. Karamanos, C. Eleftheriadis, Collapse of pressurized elastoplastic tubular members under lateral loads, International Journal of Mechanical Sciences 46 (2004) 35–56.

[7] K. Liu, K. Zhao, Z. Gao, T.X. Yu, Dynamic behavior of ring systems subjected to pulse loading, International Journal of Impact Engineering 31 (2005) 1209–1222.

[8] S.A. Karamanos, K.P. Andreadakis, Denting of internally pressurized tubes under lateral loads, International Journal of Mechanical Sciences 48 (2006) 1080–1094.

[9] E. Morris, A.G. Olabi, M.S.J. Hashmi, Analysis of nested tube type energy absorbers with different indenters and exterior constraints, Thin-Walled Structures 44 (2006) 872–885.

[10] A. Niknejad, G.H. Liaghat, H. Moslemi Naeini, A.H. Behravash, Experimental and theoretical investigation of the first fold creation in thin walled columns, Acta Mechanica Solida Sinica 23 (2010) 353–360.

[11] A. Niknejad, G.H. Liaghat, H. Moslemi Naeini, A.H. Behravash, Theoretical and experimental studies of the instantaneous folding force of the polyurethane foam-filled square honeycombs, Materials and Design 32 (2011) 69–75.

[12] A. Niknejad, M.M. Abedi, G.H. Liaghat, M. Zamani Nejad, Prediction of the mean folding force during the axial compression in foam-filled grooved tubes by theoretical analysis, Materials and Design 37 (2012) 144–151.

[13] A. Niknejad, S.A. Elahi, G.H. Liaghat, Experimental investigation on the lateral compression in the foam-filled circular tubes, Materials and Design 36 (2012) 24–34.

[14] M. Nemat-Alla, Reproducing hoop stress–strain behavior for tubular material using lateral compression test, International Journal of Mechanical Sciences 45 (2003) 605–621.

[15] Z. Fan, J. Shen, G. Lu, Investigation of lateral crushing of sandwich tubes, Procedia Engineering 14 (2011) 442–449.

[16] I.W. Hall, M. Guden, T.D. Claar, Transverse and longitudinal crushing of aluminum-foam filled tubes, Scripta Materialia 46 (2002) 513–518.

[17] A.S. Abosbaia, E. Mahdi, A.M.S. Hamouda, B.B. Sahari, A.S. Mokhtar, Energy absorption capability of laterally loaded segmented composite tubes, Composite Structures 70 (2005) 356–373.

[18] E. Mahdi, A.M.S. Hamouda, Energy absorption capability of composite hexagonal ring systems, Materials and Design 34 (2012) 201–210.

[19] J.A. Deruntz, P.G. Hodge, Crushing of a tube between rigid plates, Journal of Applied Mechanics 30 (1963) 391–398.

[20] T. Wierzbicki, W. Abramowicz, On the crushing mechanics of thin-walled structures, Journal of Applied Mechanics 50 (1983) 727–734.

[21] S.P. Santosa, T. Wierzbicki, A.G. Hanssen, M. Longseth, Experimental and numerical studies of foam-filled sections, International Journal of Impact Engineering 24 (2000) 509–534.